Molecular BioSystems

RSC Publishing

PAPER

View Article Online
View Journal | View Issue

Cite this: *Mol. BioSyst.*, 2013, **9**, 2520

Dynamical modelling of prostaglandin signalling in platelets reveals individual receptor contributions and feedback properties†

Marcel Mischnik,‡[ab] Katharina Hubertus,‡[c] Jörg Geiger,[c] Thomas Dandekar*[b] and Jens Timmer*[ade]

Received 7th April 2013,
Accepted 2nd July 2013

DOI: 10.1039/c3mb70142e

www.rsc.org/molecularbiosystems

Prostaglandins are the key-players in diminishing platelet function. They exert their effects *via* a variety of surface receptors that are linked to the cAMP/PKA-signalling cascade. However, less is known about the quantitative impact of the individual receptors on the underlying pathway. We present here a comprehensive ordinary differential equation-based model of the platelet cAMP pathway, including the four prostaglandin receptors IP, DP1, EP3 and EP4, the ADP receptor P2Y12, a detailed PKA-module as well as downstream-targets. Parameter estimation along with a comprehensive combination of time-course and dose–response measurements revealed the individual quantitative role of each receptor in elevating or decreasing pathway activity. A comparison of the two inhibiting receptors EP3 and P2Y12 exhibited a greater signalling strength of the EP3 receptor with implications for antithrombotic treatment. Furthermore, analysis of different model topologies revealed a direct influence of PKA on adenylate cyclase, reducing its maximum catalytic speed. Finally, we show here for the first time the dynamic behaviour of VASP-phosphorylation, which is commonly used as a marker for platelet-inhibition. We validate our model by comparing it to further experimental data.

Introduction

Platelets play an important role in mammalian wound healing. Their ability to aggregate and to attach to the exposed extracellular matrix is regulated by a complex network of signal-transduction pathways, including both activating and inhibiting subsets. Understanding the complex cross-regulation of these pathways is fundamental to the development of an efficient and specific anti-platelet treatment. Since blood should flow without clotting under normal physiological conditions, platelets are downregulated by default through steady cAMP/PKA-signalling. cAMP-dependent protein kinase A (PKA) repressively phosphorylates a variety of target proteins that are involved in transducing excitatory signals and performing cytoskeletal rearrangements.[1] The activation of the pathway is achieved by different classes of prostaglandins and their binding to their respective surface receptors.[2] Three prostaglandins are central to this regulation of platelet function, prostaglandin I2 (PGI2, prostacyclin), which stimulates the IP receptor, prostaglandin D2 (PGD2), which binds to the DP1 and DP2 receptors, and prostaglandin E2 (PGE2) with its receptors EP1, EP2, EP3 and EP4.[3–6] Signalling proceeds by means of activation of a stimulatory G-protein (Gs) and thus formation of cAMP by adenylate cyclase (AC). For a long time, however, the function and relevance of the PGE2 receptor EP3 remained controversial. But several pharmacological studies revealed a connection to an inhibitory G-protein (Gi),[7,8] and thus an oppositional role to the other receptors. As with EP3, the ADP receptor P2Y12 also exerts a negative effect on the pathway *via* an inhibitory G-protein. P2Y12 is also connected to PI3 kinase and plays an important role in platelet activation. Its function is disabled through the commonly applied antithrombotic drug clopidogrel.[9,10]

Despite their physiological and medical relevance, the quantitative contribution of these receptors to platelet activation and inhibition has not been shown conclusively. A previous model

[a] *Institute of physics, Hermann-herder-strasse 3a, 79104 Freiburg, Germany. E-mail: marcel.mischnik@fdm.uni-freiburg.de, jeti@fdm.uni-freiburg.de; Fax: +49 761 203 8541; Tel: +49 761 203 8532*
[b] *Department of Bioinformatics, Biocenter, Am Hubland, 97074 Wuerzburg, Germany. E-mail: dandekar@biozentrum.uni-wuerzburg.de; Fax: +49 931 888 4552; Tel: +49 931 318 4551*
[c] *Institute for Clinical Biochemistry & Pathobiochemistry, Grombühlstraße 12, 97080 Würzburg, Germany. E-mail: kathi.hubertus@gmx.de, joerg.geiger@uni-wuerzburg.de; Fax: +49 931 201 647 000; Tel: +49 931 201 47 010*
[d] *Freiburg Institute for Advanced Studies (FRIAS), Albertstrasse 19, 79104 Freiburg, Germany*
[e] *BIOSS Centre for Biological Signalling Studies, Schänzlestrasse 18, 79104 Freiburg, Germany*

† Electronic supplementary information (ESI) available. See DOI: 10.1039/c3mb70142e

‡ Equally contributing authors.

of the cAMP-pathway in platelets focused on cAMP/cGMP interplay and its regulation by phosphodiesterases, but did not include individual receptor behaviour.[11]

In the present study we model the platelet cAMP/PKA-pathway and its response to different receptors in an ordinary differential equation (ODE)-based approach. Investigation of signalling pathways by kinetic modeling is commonly applied and stimulates new biological insights into the modeled system. Combined with statistical validation based on experimental data, dynamic models can serve as a platform for testing hypotheses *e.g.* on pharmacological interventions in the system. Furthermore, the predictive features of kinetic models allow leading and directing biochemical experiments and elicit novel and unexpected biological findings. Using a data based ODE-model enables us to correctly model the behavior of measured pathway components over time as well as to test the effects of drug combinations. Experimental data used to validate our model and to fit kinetic parameters comprised both time-resolved and dose–response measurements of cAMP and the vasodilator stimulated phosphoprotein (VASP) after versatile sorts of stimuli, including activating and inhibiting agents. The reliability of the fitted parameters is examined by means of profile likelihood, a method used to determine confidence intervals and to therefore test parameter identifiabilities.[12] The model delivers kinetic constants for all involved reactions, points out individual effects of different prostaglandin receptors and shows the dynamic phosphorylation of VASP. By means of comparing the model-to-data distance different model topologies, we furthermore characterized the mechanism of AC inhibition by PKA. The fitted model is experimentally validated by additional datasets.

Results and discussion

Model set-up: topology

The input layer of the model consists of the four most important prostaglandin-receptors present on platelets, being IP, DP1, EP3 and EP4, and the ADP receptor P2Y12, with IP, DP1 and EP4 executing an elevating, and EP3 and P2Y12 administrating a moderating effect on cAMP levels, due to mobilization of either a stimulating or, in the case of EP3 and P2Y12, an inhibiting G-protein, as stated in the introduction. Thus, activation of each receptor produces a signal that is transduced to adenylate cyclase (AC). To simplify analysis, G-proteins are not included in the model. Engagement of AC leads to the production of cAMP from ATP. The ATP pool is regarded as constantly being 5 mM. The underlying kinetics is assumed to be Michaelis–Menten like. Subsequently, cAMP binds to the regulatory subunits of cAMP-dependent-protein-kinase A (PKA), which is composed of two regulatory (PKA-R) and catalytic subunits (PKA-C) each. Binding of two cAMP molecules to both PKA-Rs results in the dissociation of all 4 subunits, releasing the catalytically active PKA-Cs. Attachment of cAMPs to PKA-R is thereby reversible. After subunit-dissociation, cAMP is liberated from the free PKA-Rs. Two free PKA-Rs and PKA-Cs can finally coalesce to form one PKA tetramer. All kinetics within the PKA-module are implemented as mass–action.[13–15]

Free PKA-Cs can phosphorylate two downstream targets: the first being VASP, which is an important regulator of cytoskeletal rearrangements and one of our system's observables, the second phosphodiesterase 3A (PDE3), which degrades cAMP to AMP. Thus, a negative feedback-loop from cAMP over PKA, PDE3 and back to cAMP is established. Besides active and inactive states, PDE3 can also assume an inhibited condition *via* binding of cilostamide,[16] which represents an external driving factor in our system. The other phosphodiesterase implemented in our model is PDE2, a constitutively active enzyme. PKA-phosphorylations of VASP and PDE3, and cAMP-degradation by PDE2 and PDE3 are represented as Michaelis–Menten reactions. In addition to the downstream-targets VASP and PDE3, PKA can also repressively phosphorylate AC as an upstream target, establishing a second negative feedback-loop. The nature of this second feedback-loop will be analysed in a later section. The overall activity of AC is given by the following equation:

$$\frac{\mathrm{daAC}}{\mathrm{d}t} = \frac{\mathrm{iAC}\cdot((\mathrm{IP}_{\mathrm{act}}\cdot k_{\mathrm{IP}})+(\mathrm{DP1}_{\mathrm{act}}\cdot k_{\mathrm{DP1}})+(\mathrm{EP4}_{\mathrm{act}}\cdot k_{\mathrm{EP4}}))}{1+(\mathrm{EP3}_{\mathrm{act}}\cdot k_{\mathrm{EP3}})+(\mathrm{P2Y12}_{\mathrm{act}}\cdot k_{\mathrm{P2Y12}})} - \mathrm{aAC}\cdot k_{\mathrm{deact}}$$

aAC represents the catalytically active form, whereas iAC represents the inert enzyme. Each receptor contributes with the concentration of its ligand bound conformation and its own characteristic kinetic constant. Deactivation of adenylate cyclase is modeled as a mass-action process. Besides the activation through G-protein coupled receptors, AC can also be switched on by binding of forskolin, which represents a high-affinity allosteric activator.[17] Here, the enzyme stays in its active conformation (Fors_AC).

Ligand binding to either receptor provokes a conformational change, which renders the receptor active. K_d-values in the literature reveal in all cases an association constant, which is at least six orders of magnitude higher than the corresponding dissociation constant.[18–21] Those constants were therefore neglected. Naturally occurring steady-state situations resulting from repetitive ligand binding and dissociation cycles are reproduced within the receptors' effects on AC and its deactivation rate. EP3, EP4 and DP1 receptors are modelled as affine for PGE2, and IP for PGI2. The low affinity of IP for PGE2 was neglected.

Fig. 1 illustrates the topology of the model. Furthermore, Table S1 (ESI†) summarizes the system's signal flow. All differential equations applied are given in the ESI.†

Model set-up: kinetic parameters

Model parameters were estimated using a trust-region optimization strategy as described in the Methods section. Parameters whose values are known from literature were fixed prior to fitting. This applies for all Michaelis–Menten constants and the $V_{\max}$ values of PKA, PDE2 and PDE3. The Hill coefficient of PDE2 corresponding to 1.5 as assumed in Grant[22] was included in an initial model version, but proved to yield a larger model-to-data distance than the later applied value of 1. Receptors' affinities to their ligands were fitted likewise. The starting

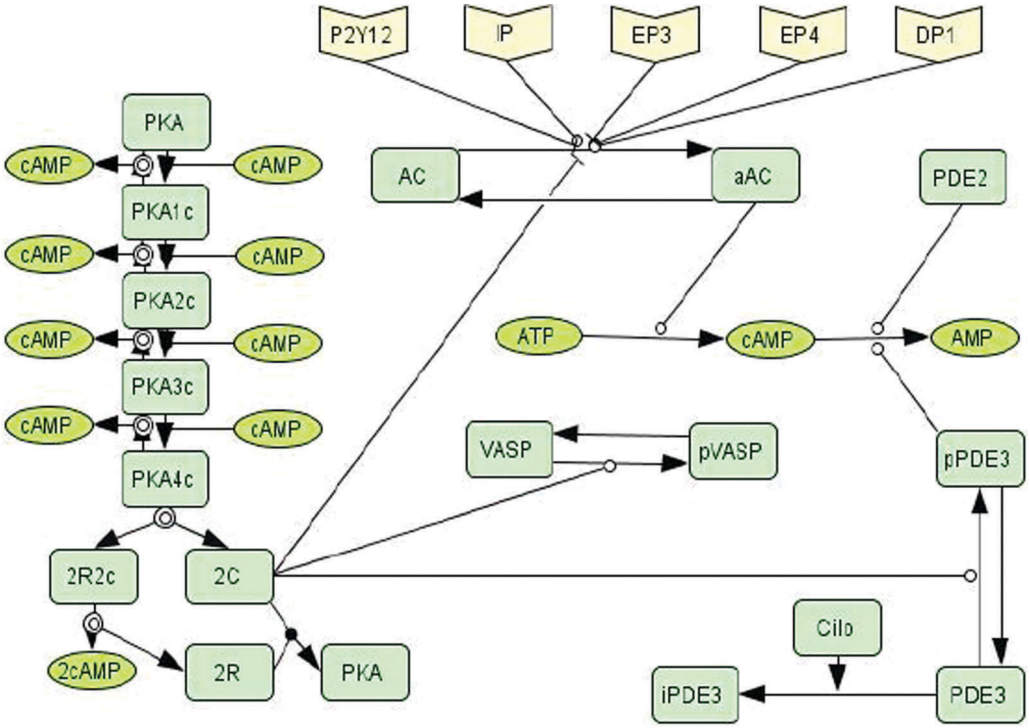

Fig. 1 Pathway topology. A receptor layer is connected to adenylate cyclase (AC) that produces cAMP upon activation. cAMP acts as a second messenger that activates the PKA-module. Free catalytic subunits phosphorylate VASP, PDE3 and AC. cAMP is degraded *via* PDE2 and 3. Arrows stand for reactions, circles represent enzymatic catalysis, blunt segments denote inhibitions and circles in circles indicate dissociations.

concentration of cAMP was determined by cAMP assay (see the Methods section), those of AC, PKA, PDE2, PDE3 and VASP were derived from mass spectroscopy data,[23] receptor concentrations were determined relatively from RNA quantifications, where the IP amount was set to 1 μM. All other initial-values were set to zero. The ESI† gives an overview of applied parameters and their origins.

Model set-up: experimental data

Measurements comprise both dose–response and time-series data after manifold combinations of stimuli. The former aim at providing information about the receptors' individual impact on cAMP signalling and are typified by detection of VASP phosphorylation (Ser157) relative to the absolute VASP-amount, after stimulation with 0.01, 1, 5, 10, 20, 50, 500 or 1000 nM of PGE2, which binds to EP3, EP4 and, with lower affinity, to DP1 (Fig. 2A). In addition, the EP4 selective antagonist L161 (5 μM) or the DP1 selective antagonist BWA (1 μM) was added in respective settings (Fig. 2B and C). Measurements were performed after 20 minutes. A comparison of Fig. 2B and C points out a biphasic activation. Whereas EP4 causes a strong increase in VASP-phosphorylation at low PGE2 concentrations, DP1 appears responsible for sustained activation at higher concentrations. The impact of the inhibitory EP3 receptor was examined by means of the selective EP3 agonist sulproston and the selective EP3 inhibitor L798. In this scenario, the cells were stimulated with 2 nM of iloprost in the presence or absence of M L798, followed by sulproston addition (10 nM) after 5 or 9 minutes. Here, cAMP was measured after 10 minutes in all cases (Fig. 2D). The impact of P2Y12 was also examined through phospho-VASP measurement. Stimulations included 1, 5, 10, 20 and 50 μM doses of ADP (Fig. 2E).

To address the dynamics of platelet cAMP signalling evoked by receptor activation, dose–response measurements are complemented by time-resolved recording of relative phospho-VASP levels, and absolute cAMP detections. VASP time-series data comprise stimulations with the direct adenylate cyclase stimulator forskolin at concentrations of 5, 10, 20, 50, 100 and 200 μM, and detection after various time points between 10 and 1800 seconds (Fig. 2F). VASP-phosphorylation reaches a steady-state at around 0.7 relative to the overall VASP amount with all applied forskolin concentrations, and maintains that level constantly. In addition, iloprost stimulations at 2 nM were conducted with both phospho-VASP and cAMP-detection (Fig. 2G). To gain information about the influence of the negative feedback-loop established by PKA and PDE3, the specific PDE3 antagonist cilostamide was added in a similar setting.

All collected data were used to fit the model parameters simultaneously (multi-experiment fitting), which, after a fit sequence of 1000 fits, yielded an overall normalized χ^2/N value of 1.01 with $N = 188$ data points. The applied initial conditions are given in the ESI† and were not changed from fit to fit. Steady-state measurements were thereby tripled with additional data points at $t = 1500$ and 1800 seconds for numerical reasons. We restricted our study to the measurement of cAMP and phosphorylated VASP, since the detection of other components

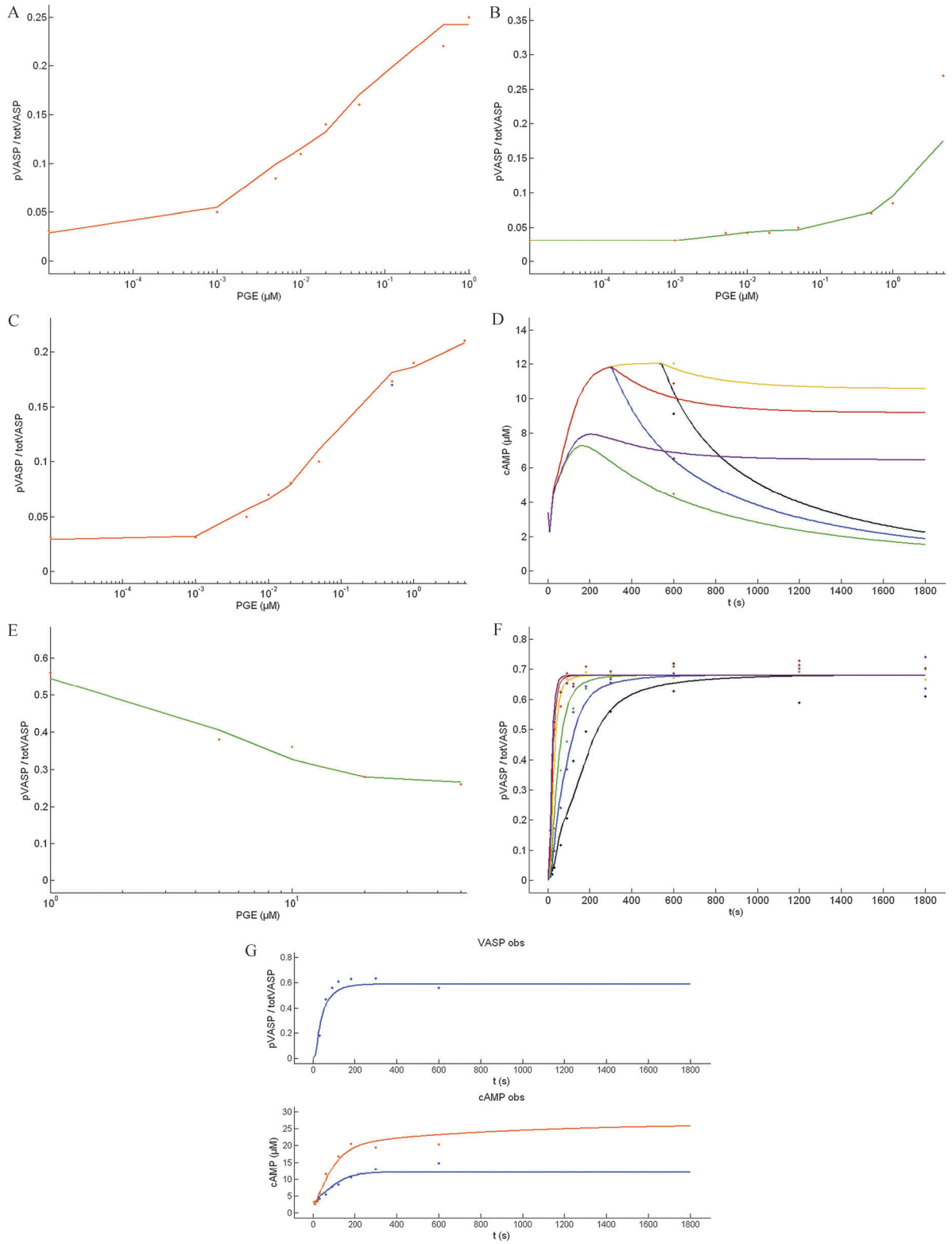

Fig. 2 Experimental data and respective model trajectories. Experimental measurements are given as points together with lines showing the calculated trajectories of the model. (A) Dose-dependent VASP-phosphorylation after PGE2-stimulation. (B) Dose-dependent VASP-phosphorylation after PGE2-stimulation in the presence of EP4-inhibitor L161 (5 μM). (C) Dose-dependent VASP-phosphorylation after PGE2-stimulation in the presence of DP1-inhibitor BWA (1 μM). (D) cAMP time-course after iloprost-stimulation combined with EP3-activation (yellow: 1 nM iloprost + 1 μM L798 + 10 nM sulproston after 540 seconds, black: 1 nM iloprost + 10 nM sulproston after 540 seconds, brown: 1 nM iloprost + 1 μM L798 + 10 nM sulproston after 300 seconds, blue: 1 nM iloprost + 10 nM sulproston after 300 seconds, purple: 1 nM iloprost + 1 μM L798 + 10 nM sulproston, green: 1 nM iloprost + 10 nM sulproston). (E) Dose-dependent VASP-phosphorylation after ADP-stimulation with iloprost pre-stimulation (1 nM). (F) Time-dependent VASP-phosphorylation after forskolin-stimulation (5, 10, 20, 50, 100 and 200 μM). (G) Time-dependent cAMP and VASP measurement after stimulation with 2 nM iloprost (blue), cAMP-measurement after iloprost-stimulation (2 nM) in the presence of 2 μM cilostamide (red). All collected data were used to fit the model parameters simultaneously.

would have been accompanied by great effort. AC for instance needs to bind the GTP-bound subunit of a G-protein in order to change its activation status. The intermediate PKA-module components on the other hand only have a very short half-life after the binding of the first cAMP molecule. As we will show later, all model parameters appear to be identifiable, even though just two players were directly measured.

Model evaluation: identifiability analysis

In our mathematical model, only two players included are observed directly. Given a model that sufficiently describes the measured data, it is important to infer how well model parameters are determined by the amount and quality of experimental data. This knowledge is essential for further investigation of model predictions. For this reason a major topic in modelling is identifiability analysis.[12]

A parameter p_i is identifiable, if the confidence interval of its estimate $\hat{p}_i$ is finite. Two different sub-types of non-identifiability can be distinguished: structural non-identifiability is adverted to the model's composition regardless of experimental data and arises from a redundant parameterization in the formal solution of $y(t)$, due to a deficient allocation of internal model states x to observables y. The set of ambiguous parameters may be varied without changing the observables $y(t)$, hence $\chi^2(p)$ remains constant.

A parameter that is structurally identifiable may still be practically non-identifiable. In contrast to structural non-identifiability, this arises frequently if the amount and the quality of experimental data are insufficient and manifests in a confidence interval that is infinitely extended in at least one direction below the applied χ^2 threshold.[12]

In our model, the profiles of all fitted parameters crossed the threshold for point-wise confidence intervals in both increasing and decreasing directions and thus proved to be identifiable (Fig. 3). Including the initial conditions into the fitting procedure would have severely diminished the parameters identifiability, even though the residuals built by the model trajectories and thus the model-to-data distance would have been smaller. Given the fact that the quantitative variability of the network components from donor to donor on the one hand and the measurement noise of the applied experimental methods on the other hand are comparatively high, we decided to go for a completely identifiable model rather than having better fits that are afflicted with uncertainties.

Model validation

To validate our model, we used two different datasets that were kept away from fitting the model. Both validations were performed using the same initial conditions as for fitting the model. The first comprised time-resolved measurements of phosphorylated VASP in the presence of the cAMP-analogue cBIMPS, which cannot be degraded by phosphodiesterases. This type of validation was applied to confirm the predicted dynamics of PKA engagement and VASP phosphorylation. Due to the slightly different affinity of cBIMPS to PKA, we introduced three new parameters, the association and dissociation constants of cBIMPS to the regulatory subunits of PKA, as well as the dissociation constant of the cBIMPS bound holoenzyme, releasing the two catalytic subunits. These parameters could not be determined based on the other data, since cBIMPS was exclusively added for validation. They thus were fitted along the new dataset, with all other parameters being fixed. As stated above, the initial conditions remained unchanged. This revealed a χ^2/N value of 0.88, with $N = 8$ data points (Fig. 4A). The model is thus able to describe the new data accurately.

The second validation comprised dose-dependent measurements of phosphorylated VASP with different concentrations of PGE2 after a pre-stimulation with iloprost. Similarly to the dose–response data used for fitting (see section Experimental data), measurements were performed 10 minutes after PGE2 was added. In this scenario, iloprost causes an elevation of VASP-phosphorylation, which gets abolished if small PGE2 concentrations are added, due to the inhibitory effect of EP3, its high affinity for PGE2, and the comparatively low activating effect of DP1 (Table 1). However, when PGE2 concentrations are increased to 200 μM and higher, the low-affinity but high impact EP4 receptor becomes engaged, which outcompetes the negative action of EP3 and raises the VASP-phosphorylation again. Fig. 4B shows the experimental data together with the respective model trajectory. Again, the model is able to describe the data ($\chi^2/N = 1.22$), even though the residuals of the model trajectory are here not entirely normally distributed. We think that despite this deviation the model is capable of yielding interesting insights into the observed system, since the overall dynamics of the measurement data could also in this case be reproduced.

Model insights: receptor effects on AC

A receptor's influence on its downstream signalling cascade is dependent on three characteristic factors: the amount of receptor molecules in the membrane, the receptor's affinity to its binding ligand, and the efficiency by which a conformational change evoked by ligand-binding is transduced to downstream targets. The first two factors are directly observable by standard biochemical techniques and are known in many cases. However, the third is dependent on detailed information about the physical structure of both the receptor molecule and the subsequent signalling components, including adaptor proteins. An aggravating fact is that, like PGE2 in our platelet system, many ligands bind to more than one receptor, which prevents a straight mapping of cellular responses to individual receptors. We therefore determined the receptors' distinct quantitative effects on their downstream target AC by means of mathematical modelling.

Similar to all other model parameters, these quantities were fitted with respect to all experimental conditions simultaneously. Due to the fact that receptor quantities are only known relatively to each other, it is not possible to infer absolute values for individual receptor contributions. However, they can be accurately given relatively to each other. Table 1 illustrates the effects of all five receptors on AC, related to an IP_AC value of 1. The upper values biochemically correspond to enzymatic

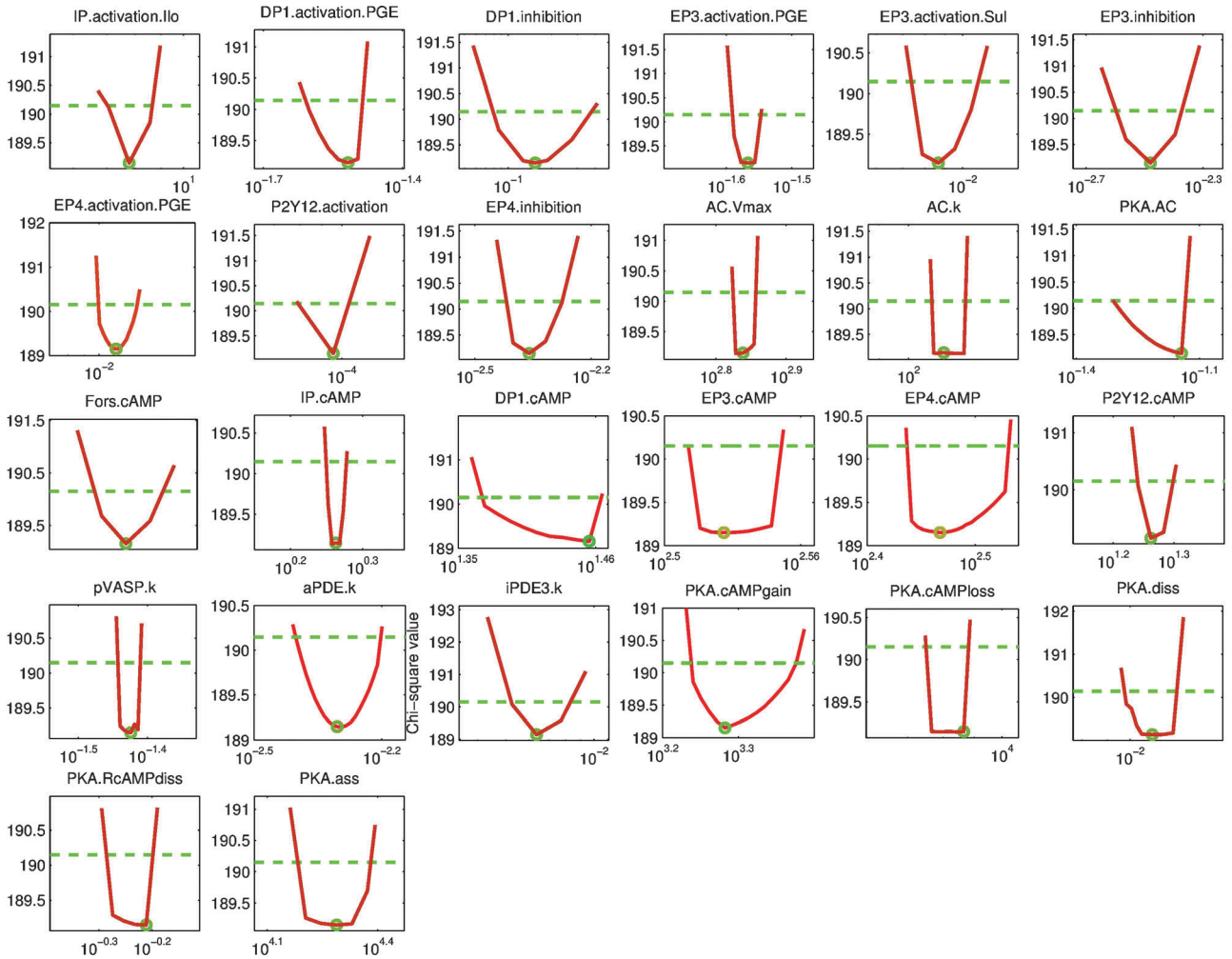

Fig. 3 Parameter profiles after a maximum of 100 re-optimization-steps in both increasing and decreasing direction. Plotted are parameter values against normalized χ^2 values. All parameters appear to be identifiable using point-wise confidence-intervals.

turnover-numbers of single receptor molecules, and have thus the dimension s^{-1}. They can be interpreted as the rate, by which a single activated receptor molecule transmits the signal *via* its G-protein to AC. It shows that, compared to IP, the effects of individual DP1 and EP4 receptors are with values of 15.57 s^{-1} and 160.28 s^{-1} much greater. Regarding inhibitory functions, P2Y12 signals with a value of 9.99 s^{-1} much weaker than EP3 (183.55 s^{-1}). The maximum signal strength transduced by the entity of a certain receptor species is also dependent on its concentration. Hence, the relative effect-parameter of each receptor (k_{ACrel}) is multiplied by its concentration in the plasma membrane in the lower row of Table 1. These values correspond to enzymatic V_{max} values. Despite the high concentration of IP, the overall effect of this receptor species (1) is still lower than that of DP1 (1.49) and EP4 (5.45). In the inhibiting group, the influence of EP3 (11.01) remains higher than that of P2Y12 (0.99), even though the concentration of EP3 is slightly lower.

The determined parameters imply medically interesting insights: since EP3 transmits its signal more efficiently than P2Y12, a pharmacological blocking of this receptor could be more effective in moderating the inhibition of cAMP signalling than the commonly used P2Y12 antagonist clopidogrel. As a consequence, the higher pathway activity would then increase the aggregation threshold for the entire cellular network and could thus counteract the effects of prothrombotic agents. However, since clopidogrel also hampers signal progression to major activating kinases like PI3 and Akt, the most effective antithrombotic strategy could be a combined approach of cAMP/PKA activation *via* EP3 blocking or EP4 activation on the one hand, and an inhibition of activating pathways on the other. Potent selective EP3 antagonists are for example ONO-240 (ref. 24) or the experimentally applied L798 (ref. 21), as selective EP4 agonists 13,14-dihydro-PGE1 (ref. 25) or ONO-4819 (ref. 26) could be named.

Model insights: PKA-feedback

In addition to the commonly known negative feedback-loop established by PDE3, previous modelling approaches[11] proposed a second feedback-loop, in which PKA directly phosphorylates AC. To characterize the nature of this second loop, we compared

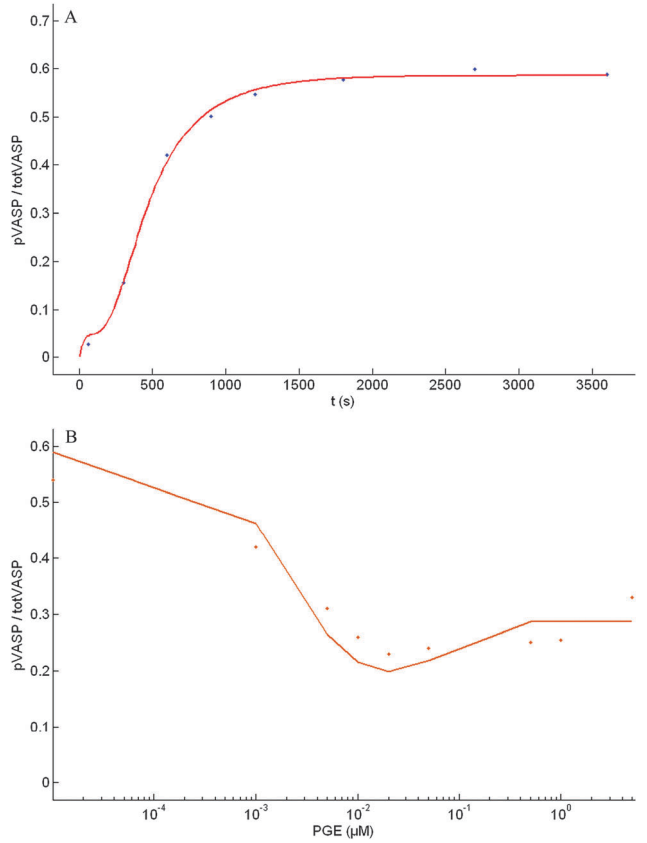

Fig. 4 Validation. (A) Time-resolved VASP-phosphorylation in the presence of 50 μM cBIMPS. Binding parameters for cBIMPS to PKA were fitted with all other parameters being fixed. (B) Dose-dependent VASP-phosphorylation after PGE2-stimulation with pre-stimulation of 2 nM iloprost.

Table 1 Receptor effect parameters related to IP

	IP	DP1	EP4	EP3	P2Y12
k_{ACrel} (relative to IP)	1	15.57	160.28	183.55	9.99
$k_{\mathrm{ACrel}}x_0$	1	1.49	5.45	11.01	0.99

different mathematical implementations (M1–M6) in terms of their ability to explain the given experimental data. For each model, a fit-sequence of 1000 fits was applied to gain the lowest possible chi-square value. The feedback-parameter k_{fb} of each model was fitted globally along with the other parameters.

In M1, the phosphorylation by PKA acts by non-competitive inhibition on the catalytic activity of AC (and Fors_AC):

$$\nu_{\mathrm{cat}} = \frac{V_{\mathrm{max}} \cdot \mathrm{ATP} \cdot \mathrm{aAC}}{(k_{\mathrm{m}} + \mathrm{ATP}) \cdot (1 + (\mathrm{PKA}/k_{\mathrm{fb}}))}$$

In M2, the feedback-loop is implemented as a factor that enhances the velocity by which an activated AC hydrolyses its GTP and is deactivated again. The deactivation rate is hence given by

$$\nu_{\mathrm{deact}} = \mathrm{aAC} \cdot (k_{\mathrm{deact}} + (\mathrm{PKA} \cdot k_{\mathrm{fb}}))$$

where aAC is the concentration of the activated cyclase, k_{deact} its regular deactivation constant and k_{fb} the strength of the feedback-loop. M3 represents a model, where k_{fb} exerts a negative effect on the activation rate of AC, analogous to the inhibiting receptors EP3 and P2Y12, *e.g.* by reducing the affinity for Gs-subunits or GTP. Here, the AC activation rate is defined by

$$\nu_{\mathrm{act}} = \frac{\mathrm{iAC} \cdot ((\mathrm{IP}_{\mathrm{act}} \cdot k_{\mathrm{IP}}) + (\mathrm{DP1}_{\mathrm{act}} \cdot k_{\mathrm{DP1}}) + (\mathrm{EP4}_{\mathrm{act}} \cdot k_{\mathrm{EP4}}))}{1 + (\mathrm{EP3}_{\mathrm{act}} \cdot k_{\mathrm{EP3}}) + (\mathrm{P2Y12}_{\mathrm{act}} \cdot k_{\mathrm{P2Y12}}) + (\mathrm{PKA} \cdot k_{\mathrm{fb}})}$$

Table 2 Model-to-data distances of selected feedback implementations

Model	Chi^2-value
M1	1.01
M2	1.61
M3	1.52
M4	1.36
M5	1.03
M6	2.05

M4 equals M3, but with PKA also acting on the Gs-independent activation through forskolin. In these two scenarios, the feedback-loop would hamper the conformational change leading to an active enzyme rather than to block Gs or GTP binding.

M5 is a combination of M1 and M4. Here, the parameter k_{fb1} influences the activation rate of AC, and k_{fb2} its catalytic activity. Both parameters were fitted with a lower bound of 10^{-5}, in order to provide that both effects are present.

M6, finally, represents the null-hypothesis, being that there is no direct influence of PKA on AC. Table 2 gives an overview over the examined feedback-implementations and their respective chi^2 values. M1 showed the smallest model-to-data distance, which implies that the negative feedback-loop by PKA exerts its function by reducing the enzyme's V_{max} and thus diminishing its catalytic activity. All other investigations were thus conducted using this feedback-implementation.

Conclusion

cAMP-signalling is an important issue in platelet function and dysfunction. We have created an ordinary differential equation-based model of platelet prostaglandin/cAMP signalling, fitted it to experimental data and validated the results by additional datasets. Our data show for the first time the dynamic behaviour of VASP-phosphorylation after various stimulation types, which could be accurately reproduced by modelling. Furthermore, we mathematically determined the individual receptor contributions to cAMP signalling and examined a possible second negative feedback-loop established by PKA *via* adenylate cyclase phosphorylation, which could not only be confirmed, but also further characterized. We examined the reliability of our model by means of profile-likelihood-based identifiability analysis. Our approach shows the EP3 and EP4 receptors to be important targets. Efficient pharmacological modulation of either could have a greater effect on antithrombotic cAMP signalling than P2Y12 antagonists such as clopidogrel. A prolonged activation of the cAMP pathway (or a block of its inhibition) would be a novel means to prevent inappropriate

platelet activation, and may thus complement classical approaches. The obtained information is a further step to understanding the complex signalling processes that constitute the basis for thrombocyte-based wound-healing, and permit improved pharmacological modulation of platelets with application potential both in thrombotic diseases and coagulopathies as well as in acute and chronic inflammatory action of platelets. Drugs modulating the intracellular cAMP concentration in platelets have been proven efficient platelet inhibitors with minor side-effects. Current anti-aggregatory drug development is mainly aimed at these pathways. However experience with these novel drugs has indicated a wide variability in their efficacy, which may result from genetic predisposition, co-medication or other, yet unknown reasons. By combination of appropriate drugs these shortcomings may be overcome. To enable adequate medication detailed knowledge of the underlying mechanisms and their particular contribution to signalling is of fundamental importance. Both, drug development and future therapeutic strategies will benefit from a quantitative model of the signalling pathways.

Methods

Computational methods

***In silico* modelling.** The model consists of a set of ordinary differential equations, representing concentration changes over time. Rate constants taken from the literature all arise from studies on human platelets. The basal model incorporated mass action, Michaelis–Menten and custom kinetics. It was optimized by fitting it 1000 times to all available experimental data simultaneously (multi-experiment-fitting), each time varying all parameters with a disturbance strength s of 0.3 corresponding to $p_{new} = p_{old} \times 10^{(s \times u)}$ with u being normally distributed with mean 0 and variance 1. Since we applied multi-experiment-fitting, the same initial conditions were used for all experimental scenarios. The magnitude of the measurement error was estimated along with the remaining parameters. Therefore, a parameterized error model of the form

$$\varepsilon_{tot} = \varepsilon_{rel} y + \varepsilon_{relmax} \max(y)$$

describing the measurement noise was assumed. The type of the error is Gaussian. The additional parameters ε_{rel} and ε_{relmax} accounting for relative noise and noise relative to the maximum were estimated simultaneously with the other model parameters.

Corresponding differential equations were implemented and further analyzed using the MATLAB toolbox PottersWheel.[27]

Parameter estimation. Determining model parameters that optimize the merit function and set the model statistically compliant with the available data is a fundamental problem. To fit the model

$$y = y(t_i, \vec{p})$$

to data, we optimize the χ^2-merit function

$$\chi^2(\vec{p}) = \sum \frac{y_i - y(t_i, \vec{p})}{\sigma^2}$$

with y_i representing data point i with standard deviation σ_i. The model value at time point i for a set of parameter values $\vec{p}$ is given by $y(t_i, \vec{p})$. Assuming normally distributed measurement errors, this corresponds to a maximum likelihood estimation. To optimize this function, we used the trust region algorithm in the logarithmic parameter space,[28] a powerful deterministic least-square optimizer. ODE-integration was thereby performed by means of SVODES.[29]

Profile-likelihood estimation. The idea of profile likelihood estimation is to explore the parameter space for each parameter in the direction of the least increase in χ^2. It can be calculated for each parameter individually by

$$\chi_{PL}^2(p_i) = \min_{p_{j \neq i}} [\chi^2(p)]$$

meaning re-optimization of $\chi^2(p)$ with respect to all parameters $p_{j \neq i}$, for each value of parameter p_i. Hence, the profile likelihood keeps χ^2 as small as possible alongside p_i. Structural non-identifiable parameters are characterized by a flat profile likelihood. The profile likelihood of a practically non-identifiable parameter has a minimum, but it does not exceed a threshold α for increasing and/or decreasing values of p_i. In contrast, the profile likelihood of an identifiable parameter exceeds α for both increasing and decreasing values of p_i. The points of passover represent likelihood-based confidence intervals.[12]

Experimental methods

Platelet preparation. Platelets were used as washed platelets (WP) resuspended in phosphate buffered saline (PBS, 137 mM NaCl, 2.7 mM KCl, 10 mM Na_2HPO_4, 2 mM KH_2PO4, pH = 7.4), depending on the assay applied, and prepared from whole human blood as described elsewhere[30] with modifications to avoid contamination by other cells. Whole human blood was obtained from healthy volunteers who had not taken any medication affecting platelet function within 2 weeks prior to the experiment after informed consent according to the declaration of Helsinki and our institutional guidelines and as approved by the local ethics committee. The blood was drawn by venipuncture and collected in 1/5 volume of HEPES–citrate buffer (120 mM NaCl, 20 mM sodium citrate, 4 mM KCl, 1.5 mM citric acid, 30 mM D-glucose, 8 mM HEPES, pH = 6.5) and centrifuged at 300 × g for 20 minutes at 20 °C to obtain platelet rich plasma (PRP). For the preparation of washed platelets the PRP was diluted 1 : 1 with HEPES–citrate buffer, apyrase (1 U ml^{-1}) added and centrifuged again at 100 × g for 10 min at 20 °C. The pellet was discarded and the supernatant was centrifuged at 380 × g for 10 minutes. The resulting pellet was resuspended in HEPES/citrate, left resting for 5 minutes and centrifuged again at 380 × g for 10 minutes. The platelet pellet was resuspended in PBS buffer to a cell density of 3 × 10^8 platelets per ml and apyrase (0.1 U ml^{-1}) added. Washed platelets were used in 200 μl portions. The samples were incubated with the reagents in the water bath at 37 °C as indicated, stopped and treated appropriately for the respective analyte. The reagents were solved in PBS unless otherwise stated.

Table 3 Receptor quantifications

Receptor	Amount (relative to IP)
IP	1
DP1	0.096
EP3	0.06
EP4	0.034
P2Y12	0.1

cDNA preparation. Total RNA was isolated from WP using the Trizol method according to the manufacturer's protocol (Invitrogen, Darmstadt, Germany). WP were centrifuged to produce a pellet containing 3.5×10^8 platelets, which was resuspended in 1 ml of Trizol. To visualize the pellet, 2 μl 3 M sodium acetate was added. After the addition of 400 μl chloroform the suspension was mixed well and incubated for 5 minutes on ice. The suspension was centrifuged (4 °C, 9000 × *g*, 10 minutes) and the upper phase was transferred to a tube, 600 μl ice-cold isopropanol added and centrifuged (4 °C, 9000 × *g*, 15 minutes) again. The pellet was resuspended in 1 ml 70% ethanol and centrifuged (4 °C, 9000 × *g*, 15 minutes). The supernatant was discarded and the pellet was dried and resuspended in 10 μl de-ionised water. mRNA was transcribed in cDNA by the reverse transcriptase reaction with SuperScript II (Invitrogen, Darmstadt, Germany). The platelet cDNA was tested against leukocyte and genomic contamination with specific oligonucleotides and only used if tests were negative. Human normal tissues cDNA (BioChain) was used as positive control. The oligonucleotides were designed against all known isoforms of the receptors. Quantitative PCR was done with Platinum Taq Polymerase. All PCR products were validated by sequencing. Table 3 shows the determined relative receptor amounts.

cAMP EIA. Cyclic adenosine 5′-monophosphate (cAMP) determination was carried out as described in ref. 30. In brief, platelets were lysed with the original volume of 70%(v/v) ice cold ethanol and kept on ice for 30 minutes. The precipitate was removed by centrifugation for 10 minutes at 10 000 × *g* and 4 °C and washed again with the same volume of 70%(v/v) ethanol. The ethanol extracts were combined and dried in the vacuum. The dried samples were dissolved in 200 μl of the assay buffer supplied with the assay and acetylated to increase assay sensitivity as described in ref. 30. The samples were measured in a Wallac Victor 1420 (Perkin-Elmer) plate reader at 405 nm. Sample readings below 30% or above 70% $\%B/B_0$ are off the dynamic range of the assay and were repeated with an appropriate dilution of the sample.

VASP phosphorylation. VASP phosphorylation is a highly sensitive indicator for platelet cAMP regulation.[30] We determined VASP phosphorylation in a solid-phase assay either by VASP binding on a zyxin matrix[30] or in a sandwich ELISA (BioCytex, Marseille, France).[31] The zyxin matrix pVASP assay was carried out as described elsewhere.[30] Platelet samples (200 μl each) were lysed by addition of an equal volume of ice cold lysis buffer (20 mM Tris-HCl, 150 mM NaCl, 1 mM EDTA, 1 mM EGTA, 1% Triton X-100, 0.5% NP-40, 10 mM β-glycerol-phosphate, 10 mM NaF, pH = 7.4) and thorough mixing on a vortex mixer. The samples were diluted with PBS buffer by 1 : 10. Each sample was measured in triplicate for the VASP phospho-Ser157 antibody (5C6) and total VASP antibody (IE273). As control for background and non-specific binding 5% bovine serum albumin (BSA) solved in lysis buffer was used. 100 μl sample per well of the zyxin coated microtiter plate were incubated for 1 h at room temperature under shaking and washed three times with 300 μl per well PBS-T (0.1% Tween20 supplemented PBS), 1 h incubated with the primary antibodies, washed 3 times with PBS-T, the secondary antibody (horse radish peroxidase coupled goat anti-mouse IgG) added, incubated and washed as mentioned above. The detection reagent ABTS was added, incubated for 20 minutes at room temperature under shaking and the absorbance of the samples was measured in the microtiter plates with a Wallac Victor 1420 (Perkin-Elmer) plate reader at 405 nm each for 1 second. From the absorbance of each sample the absorbance of the background control sample for the respective antibody was subtracted, and the resulting data were multiplied by the dilution factor. From the values obtained with the phosphospecific and the total VASP antibodies the phospho-VASP/VASP ratio was calculated.

Acknowledgements

This work was funded by the German Federal Ministry of Education and Research, Project SARA (FKZ 0315395B,C,E). We thank Dr U. Rapp-Galmiche for stylistic suggestions and native speaker corrections.

Notes and references

1 A. Smolenski, *J. Thromb. Haemostasis*, 2012, **10**(2), 167–176.
2 R. C. Jin, B. Voetsch and J. Loscalzo, *Microcirculation*, 2005, **12**(3), 247–258.
3 H. Wise, Y. H. Wong and R. L. Jones, *Neurosignals*, 2002, **11**(1), 20–28.
4 S. Kuriyama, H. Kashiwagi, K. Yuhki, F. Kojima, T. Yamada and T. Fujino, *et al.*, *Thromb. Haemostasis*, 2010, **104**(4), 796–803.
5 R. J. Gryglewski, *Pharmacol. Rep.*, 2008, **60**(1), 3–11.
6 E. Lai, L. A. Wenning, T. M. Crumley, I. De Lepeleire, F. Liu and J. N. de Hoon, *et al.*, *Clin. Pharmacol. Ther.*, 2008, **83**(6), 840–847. Epub 2007 Sep 19.
7 S. Heptinstall, D. I. Espinosa, P. Manolopoulos, J. R. Glenn, A. E. White and A. Johnson, *et al.*, *Platelets*, 2008, **19**(8), 605–613.
8 J. Singh, W. Zeller, N. Zhou, G. Hategen, R. Mishra and A. Polozov, *et al.*, *ACS Chem. Biol.*, 2009, **4**(2), 115–126.
9 J. Geiger, P. Hönig-Liedl, P. Schanzenbächer and U. Walter, *Eur. J. Pharmacol.*, 1998, **351**(2), 235–246.
10 P. Savi, C. Labouret, N. Delesque, F. Guette, J. Lupker and J. M. Herbert, *Biochem. Biophys. Res. Commun.*, 2001, **283**(2), 379–383.
11 G. Wangorsch, E. Butt, R. Mark, K. Hubertus, J. Geiger, T. Dandekar and M. Dittrich, *BMC Syst. Biol.*, 2011, **5**, 178.

12 A. Raue, C. Kreutz, T. Maiwald, J. Bachmann, M. Schilling, U. Klingmüller and J. Timmer, *Bioinformatics*, 2009, **25**(15), 1923–1929.
13 U. Walter, M. Eigenthaler, J. Geiger and M. Reinhard, *Adv. Exp. Med. Biol.*, 1993, **344**, 237–249.
14 S. S. Taylor, J. A. Buechler, L. W. Slice, D. K. Knighton, S. Durgerian and G. E. Ringheim, *et al.*, *Cold Spring Harbor Symp. Quant. Biol.*, 1988, **53**(Pt 1), 121–130.
15 K. Taskén, B. S. Skålhegg, K. A. Taskén, R. Solberg, H. K. Knutsen and F. O. Levy, *et al.*, *Adv. Second Messenger Phosphoprotein Res.*, 1997, **31**, 191–204.
16 M. Endoh, K. Satoh and S. Yamashita, *Eur. J. Pharmacol.*, 1980, **66**(1), 43–52.
17 R. H. Alasbahi and M. F. Melzig, *Pharmazie*, 2012, **67**(1), 5–13.
18 M. Abramovitz, M. Adam, Y. Boie, M. Carrière, D. Denis and C. Godbout, *et al.*, *Biochim. Biophys. Acta*, 2000, **1483**(2), 285–293.
19 D. H. Wright, K. M. Metters, M. Abramovitz and A. W. Ford-Hutchinson, *Br. J. Pharmacol.*, 1998, **123**(7), 1317–1324.
20 R. J. Wilson, G. M. Giblin, S. Roomans, S. A. Rhodes, K. A. Cartwright and V. J. Shield, *et al.*, *Br. J. Pharmacol.*, 2006, **148**, 326–339.
21 H. Juteau, Y. Gareau, M. Labelle, C. F. Sturino, N. Sawyer and N. Tremblay, *et al.*, *Bioorg. Med. Chem.*, 2001, **9**, 1977–1984.
22 P. G. Grant, A. F. Mannarino and R. W. Colman, *Thromb. Res.*, 1990, **59**(1), 105–119.
23 J. M. Burkhart, M. Vaudel, S. Gambaryan, S. Radau, U. Walter and L. Martens, *et al.*, *Blood*, 2012, **120**(15), e73–e82.
24 H. Amano, I. Hayashi, H. Endo, H. Kitasato, S. Yamashina and T. Maruyama, *et al.*, *J. Exp. Med.*, 2003, **197**, 221–232.
25 T. L. Davis and N. A. Sharif, *Br. J. Pharmacol.*, 2000, **130**, 1919–1926.
26 K. Yoshida, H. Oida, T. Kobayashi, T. Maruyama, M. Tanaka, T. Katayama and K. Yamaguchi, *et al.*, *Proc. Natl. Acad. Sci. U. S. A.*, 2002, **99**, 4580–4585.
27 T. Maiwald and J. Timmer, *Bioinformatics*, 2008, **24**(18), 2037–2043.
28 T. F. Coleman and Y. Li, *SIAM J. Control*, 1996, **6**, 418–445.
29 A. C. Hindmarsh, P. N. Brown, K. E. Grant, S. L. Lee, R. Serban and D. E. Shumaker, *et al.*, *ACM Trans. Math. Software*, 2005, **31**(3), 396.
30 J. Geiger, T. Brandmann, K. Hubertus, B. Tjahjadi, R. Schinzel and U. Walter, *Anal. Biochem.*, 2010, **407**(2), 261–269.
31 P. Barragan, F. Paganelli, L. Camoin-Jau and N. Bourguet, *Thromb. Haemostasis*, 2010, **104**(2), 410–411.